JOURNAL OF SOLID STATE CHEMISTRY **134,** 382–387 (1997)
ARTICLE NO. SC977597

Effect of Spin State of Ni^{3+} Ions on Electrical Properties of $Nd(Cr_{1-x}Ni_x)O_3$

Hideki Taguchi

Research Laboratory for Surface Science, Faculty of Science, Okayama University, Okayama 700, Japan

Received February 4, 1997; in revised form August 6, 1997; accepted August 19, 1997

Orthorhombic perovskite-type $Nd(Cr_{1-x}Ni_x)O_3$ ($0.0 \leq x \leq 0.6$) was synthesized in a flow of pure oxygen gas. Magnetic measurement indicates that the $1/\chi$–T curves of $Nd(Cr_{1-x}Ni_x)O_3$ are linear and have deflection points (≈ 480 K) in the range $0.2 \leq x \leq 0.6$. Measurements of the electrical resistivity (ρ) and the Seebeck coefficient (α) indicate that $Nd(Cr_{1-x}Ni_x)O_3$ ($0.0 \leq x \leq 0.4$) is a p-type semiconductor, while $Nd(Cr_{0.4}Ni_{0.6})O_3$ ($x = 0.6$) is an n-type semiconductor. $\log \rho$–$1000/T$ curves are linear and have the deflection points at ≈ 500 K ($0.2 \leq x \leq 0.6$). Calculation of the activation energy (E_a) indicates that E_a ($300 \leq T \leq 500$ K) is slightly lower than E_a ($500 \leq T \leq 900$ K). From these results, it is obvious that the electrical properties are strongly affected by the spin state of the Ni^{3+} ion.

INTRODUCTION

$NdCrO_3$ has an orthorhombic perovskite-type structure with $a = 0.5430$ nm, $b = 0.7692$ nm, and $c = 0.5488$ nm and exhibits antiferromagnetism with a Néel temperature (T_N) of 224 K (1, 2). Magnetic measurement indicates that the electron configuration of the Cr^{3+} ion is $(d\varepsilon)^3(d\gamma)^0$. $NdCrO_3$ is a p-type semiconductor above room temperature, and the activation energy (E_a) calculated from the linear portion of the $\log \rho$–$1000/T$ curve is ≈ 0.28 eV (3, 4). Rao *et al.* reported that orthorhombic perovskite-type $LaCrO_3$ is a p-type semiconductor, and three $3d$ electrons of the Cr^{3+} ion exist in the localized t_{2g}^* level (3). Since the ionic radius and the electronegativity of the La^{3+} ion are nearly equal to those of the Nd^{3+} ion, the band structure of $NdCrO_3$ is considered to resemble the band structure of $LaCrO_3$ (5, 6).

High oxygen pressure (above 20 MPa) is necessary to synthesize stoichiometric $RNiO_3$ (R = La, Sm, Nd, etc.) (7–9). $NdNiO_3$ has the orthorhombic perovskite-type structure with $a = 0.5378$ nm, $b = 0.7608$ nm, and $c = 0.5390$ nm and exhibits a metal–insulator transition at 200 K (7, 10). $NdNiO_3$ is an n-type semiconductor below 200 K and is metallic above 200 K. Frand *et al.* reported that the transition temperature of $(Sm_{1-x}Nd_x)NiO_3$ ($0.0 \leq x \leq 1.0$) decreases with increasing x (8). From these results, it is considered that the metal–insulator transition would result from the band gap closing and eventually from O($2p$) and Ni($3d$) band overlapping that occurs because of the lattice contraction at low temperature (11). Although rhombohedral $LaNiO_3$ is metallic in the entire temperature range, it decomposes into La_2NiO_4 and NiO above 1223 K (7, 9).

The electrical conductivity of $NdCrO_3$ is assumed to occur by the thermal excitation of the $3d$ electrons from the t_{2g}^* level to the e_g^* level. Since there are more than three $3d$ electrons in $Nd(Cr_{1-x}Ni_x)O_3$, the $3d$ electrons would exist in both the t_{2g}^* and the e_g^* levels. Therefore, it is assumed that the electrical conductivity may increase with increasing x. In the present study, $Nd(Cr_{1-x}Ni_x)O_3$ ($0.0 \leq x \leq 0.6$) was synthesized in a flow of pure oxygen gas (0.1 MPa) to refine its structure and to measure the electrical resistivity, the Seebeck coefficient, and the magnetic properties. These results will provide information regarding the cation–anion–cation overlap in orthorhombic perovskite-type $Nd(Cr_{1-x}Ni_x)O_3$.

EXPERIMENTAL

$Nd(Cr_{1-x}Ni_x)O_3$ ($0.0 \leq x \leq 0.6$) was prepared by a standard ceramic technique. $Nd(NO_3)_3 \cdot 6H_2O$ (Kanto Chemical Co. Inc., Tokyo, Japan, 99.95%), Cr_2O_3 (Nacalai tesque, Kyoto, Japan, guaranteed grade reagent), and $Ni(CH_3COO)_2 \cdot 4H_2O$ (Nacalai tesque, Kyoto, Japan, guaranteed grade reagent) powders were weighed in the appropriate proportions and milled with acetone. After the mixed powders were dried at 343 K, they were calcined at 673 K for a few hours in air and then fired 1323 K for 24 h in a flow of pure oxygen gas. To measure the electrical properties, the powders were pressed into a pellet form under a pressure of 50 MPa, and the pellet was sintered at 1323 K for 12 h in the flow of pure oxygen gas.

The phases of the samples were identified by X-ray powder diffraction (XRD) with monochromatic Cu$K\alpha$ radiation. The structure refinement was carried out by Rietveld analysis of the XRD data with the RIETAN program written by Izumi (12). XRD data were collected by step scanning

0022-4596/97 $25.00

over the angular range $20^\circ \leq 2\theta \leq 100^\circ$ in increments of 0.02° (2θ) with monochromatic Cu$K\alpha$ radiation.

The oxygen content of the samples was determined by an oxidation–reduction (redox) method (13). The sample ($\approx$100 mg) was weighted and put into a conical beaker. Both a 0.1 N aqueous solution (20 cm^3) of sodium oxalate and 10 cm^3 of perchloric acid (60%) were added to the beaker. To dissolve the sample, the beaker was heated in a flow of carbon dioxide gas. After the beaker was cooled to room temperature, the solution was titrated with a 0.02 N aqueous solution of potassium permanganate. The electrical resistivity (ρ) of the samples was measured by a standard four-electrode technique in the temperature range $300 \leq T \leq 973$ K. The Seebeck coefficient (α) was measured in the temperature range $300 \leq T \leq 973$ K (14), and the heating rate was 1 K/min. The magnetic susceptibility (χ) was measured by a magnetic torsion balance in the temperature range $300 \leq T \leq 673$ K. The density of the sintered samples was measured by means of the water displacement method.

RESULTS AND DISCUSSION

XRD patterns of $Nd(Cr_{1-x}Ni_x)O_3$ ($0.0 \leq x \leq 0.6$) were completely indexed as the orthorhombic perovskite-type structure. I tried to dissolve $Nd(Cr_{1-x}Ni_x)O_3$ by perchloric acid for the determination of the oxygen content. However, it was impossible to dissolve $Nd(Cr_{1-x}Ni_x)O_3$ ($0.0 \leq x \leq 0.4$) except $Nd(Cr_{0.4}Ni_{0.6})O_3$ ($x = 0.6$). The oxygen content of $Nd(Cr_{0.4}Ni_{0.6})O_3$ ($x = 0.6$) was determined to be 2.97. Since the Cr^{3+} ion is very stable in metal oxides (Cr_2O_3, $LaCrO_3$, $YCrO_3$, etc.) and $Nd(Cr_{0.4}Ni_{0.6})O_3$ ($x = 0.6$) has only a slight oxygen deficiency, we admit in the following that the oxygen deficiency of $Nd(Cr_{1-x}Ni_x)O_3$ is negligible in the range $0.0 \leq x \leq 0.6$.

Assuming that $Nd(Cr_{1-x}Ni_x)O_3$ ($0.0 \leq x \leq 0.6$) has the orthorhombic $GdFeO_3$-type structure with space group *Pnma*, the structure refinement was carried out by Rietveld analysis of XRD data (15). Isotropic thermal parameters (B) for Nd, Cr, Ni, O(1), and O(2) ions were fixed at 0.003 nm^2 for all samples. Refined structural parameters and residuals R_{WP}, R_I, and R_F are listed in Table 1. R_{WP}, R_I, and R_F are the weighted pattern, the integrated intensity, and the structure factor, respectively. The final R_F of all samples is less than 1.29%, and the low R_F suggests that the structural model for $Nd(Cr_{1-x}Ni_x)O_3$ is reasonable. As shown in Fig. 1, the observed XRD pattern for $Nd(Cr_{0.4}Ni_{0.6})O_3$ ($x = 0.2$) agrees very well with the calculated XRD pattern.

Figure 2 shows the relationship between the cell constants (a-, b-, and c-axes) of $Nd(Cr_{1-x}Ni_x)O_3$ ($0.0 \leq x \leq 0.6$) and the composition (x). In Fig. 2, the cell constants of $NdNiO_3$ ($x = 1.0$) reported by Alonso *et al.* are also plotted as filled circles (7). Both the b- and c-axes decrease with increasing x, while the a-axis has a maximum value at $x = 0.2$–0.4. In $Nd(Cr_{1-x}Ni_x)O_3$ ($0.0 \leq x \leq 0.6$), A-site cations (Nd ions) coordinate with twelve anions, four O(1) and eight O(2) ions. B-site cations (Cr and Ni ions) coordinate with six anions, two O(1) and four O(2) ions. Table 2 shows the (Cr,Ni)–O(1 and 2) distances calculated from the refined structural parameters and the Ni–O(1 and 2) distances of $NdNiO_3$ ($x = 1.0$) reported by Alonso *et al.* (7). The (Cr,Ni)–O(1 and 2) distances are almost independent of x in the range $0.0 \leq x \leq 0.4$ and then decreases with increasing x in the range $0.4 \leq x \leq 1.0$. The angles for O(1)–(Cr,Ni)–O(1), O(1)–(Cr,Ni)–O(2), and O(2)–(Cr,Ni)–O(2) is 180°, 90°, and 90° or 180°, respectively. Table 3 shows the angles for (Cr,Ni)–O(1 and 2)–(Cr,Ni) calculated from the refined structure and the angles for Ni–O(1 and 2)–Ni of $NdNiO_3$ ($x = 1.0$) reported by Alonso *et al.* (7). The angles for (Cr,Ni)–O(1 and 2)–(Cr, Ni) are less than 180°, and the angle for (Cr,Ni)–O(1)–(Cr,Ni) has the minimum value at $x = 0.2$–0.4. On the other hand, the angle for (Cr,Ni)–O(2)–(Cr,Ni) increases linearly with increasing x.

Figure 3 shows the relationship between the inverse magnetic susceptibility ($1/\chi$) of $Nd(Cr_{1-x}Ni_x)O_3$ ($0.0 \leq x \leq 0.6$) and temperature. $Nd(Cr_{1-x}Ni_x)O_3$ ($0.0 \leq x \leq 0.6$) is paramagnetic and the $1/\chi$–T curves are linear in the temperature range $300 \leq T \leq 673$ K. The deflection points ($\approx$480 K) in the $1/\chi$–T curves are observed in the range $0.2 \leq x \leq 0.6$

TABLE 1
Refined Structure Parameters of $Nd(Cr_{1-x}Ni_x)O_3$

Atom	Position	x	y	z	B
$x = 0.0$	$a = 0.54798(1)$ nm	$b = 0.76918(2)$ nm	$c = 0.54221(1)$ nm		
	$R_{WP} = 12.69\%$	$R_I = 2.01\%$	$R_F = 1.29\%$		
Nd	4(*c*)	0.041(1)	0.25	− 0.008(1)	0.003
Cr	4(*b*)	0	0	0.5	0.003
O(1)	4(*c*)	0.484(4)	0.25	0.082(6)	0.003
O(2)	8(*d*)	0.292(4)	0.041(3)	− 0.289(4)	0.003
$x = 0.2$	$a = 0.54890(1)$ nm	$b = 0.76877(2)$ nm	$c = 0.54167(1)$ nm		
	$R_{WP} = 11.69\%$	$R_I = 1.66\%$	$R_F = 1.06\%$		
Nd	4(*c*)	0.043(1)	0.25	− 0.009(1)	0.003
Cr,Ni	4(*b*)	0	0	0.5	0.003
O(1)	4(*c*)	0.482(4)	0.25	0.085(5)	0.003
O(2)	8(*d*)	0.291(3)	0.039(3)	− 0.289(4)	0.003
$x = 0.4$	$a = 0.54899(1)$ nm	$b = 0.76754(2)$ nm	$c = 0.54093(1)$ nm		
	$R_{WP} = 12.46\%$	$R_I = 2.16\%$	$R_F = 1.25\%$		
Nd	4(*c*)	0.045(1)	0.25	− 0.010(1)	0.003
Cr,Ni	4(*b*)	0	0	0.5	0.003
O(1)	4(*c*)	0.483(4)	0.25	0.086(5)	0.003
O(2)	8(*d*)	0.292(3)	0.038(3)	− 0.290(4)	0.003
$x = 0.6$	$a = 0.54642(2)$ nm	$b = 0.76586(3)$ nm	$c = 0.54050(2)$ nm		
	$R_{WP} = 13.10\%$	$R_I = 2.25\%$	$R_F = 1.08\%$		
Nd	4(*c*)	0.043(1)	0.25	− 0.009(1)	0.003
Cr,Ni	4(*b*)	0	0	0.5	0.003
O(1)	4(*c*)	0.485(4)	0.25	0.077(6)	0.003
O(2)	8(*d*)	0.289(4)	0.036(3)	− 0.293(4)	0.003

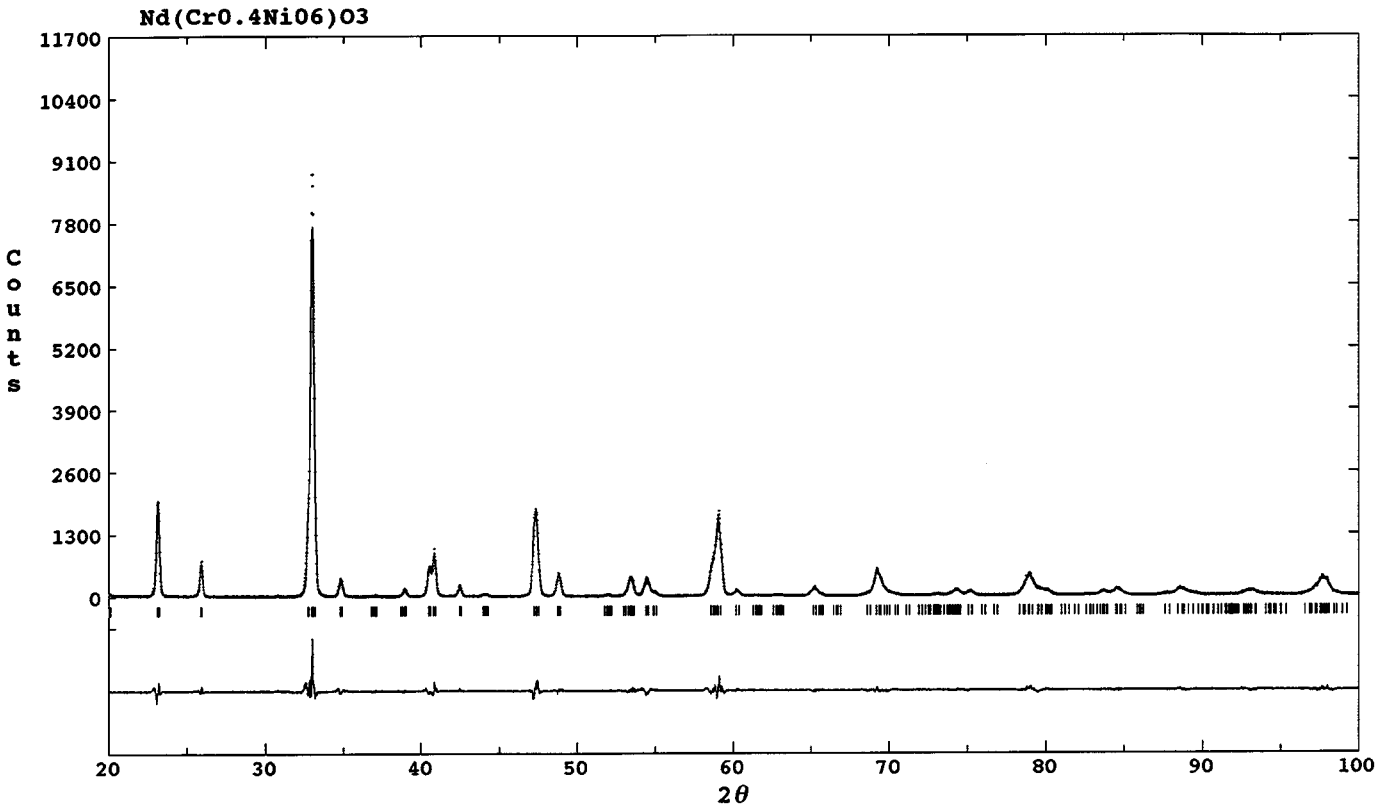

FIG. 1. Observed XRD pattern with the difference between the observation and calculation for $Nd(Cr_{0.4}Ni_{0.6})O_3$ ($x = 0.6$).

and shown as arrows in Fig. 3. Figure 4 shows the effective magnetic moment (μ_{eff}) of $Nd(Cr_{1-x}Ni_x)O_3$ calculated from the linear portions in the $1/\chi$–T curves. In Fig. 4, the open circles and the open triangles indicate the observed μ_{eff} ($300 \leq T \leq 480$ K) and the observed μ_{eff} ($480 \leq T \leq 650$ K), respectively. The theoretical μ_{eff} is calculated using the following equation:

$$\mu_{eff} = \sqrt{(1-x)\mu^2_{Cr^{3+}} + x\mu^2_{Ni^{3+}} + \mu^2_{Nd^{3+}}}, \qquad [1]$$

where $\mu_{Cr^{3+}}$, $\mu_{Ni^{3+}}$, and $\mu_{Nd^{3+}}$ are the effective magnetic moments of the Cr^{3+} ion, the Ni^{3+} ion, and the Nd^{3+} ion,

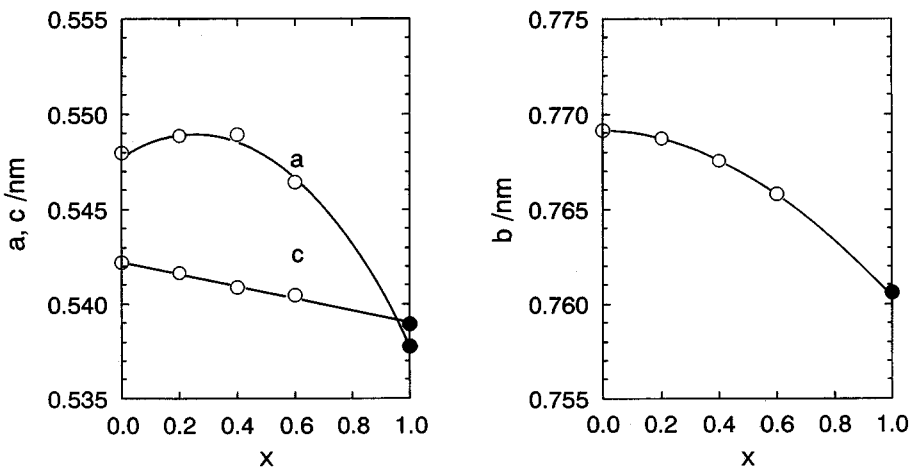

FIG. 2. Cell constants vs composition (x) for the system $Nd(Cr_{1-x}Ni_x)O_3$. Filled circles indicate the cell constants of $NdNiO_3$ ($x = 1.0$) reported by Alonso *et al.* (7).

TABLE 2
(Cr,Ni)–O(1 and 2) Distances of $Nd(Cr_{1-x}Ni_x)O_3$

x	(Cr,Ni)–O(1) × 2 nm	(Cr,Ni)–O(2) × 2 nm	(Cr,Ni)–O(2) × 2 nm
0.0	0.1976(7)	0.1961(21)	0.1993(21)
0.2	0.1979(7)	0.1964(19)	0.1987(19)
0.4	0.1976(6)	0.1962(19)	0.1987(19)
0.6	0.1961(7)	0.1955(25)	0.1978(24)
1.0[a]	0.1940(1)	0.1939(2)	0.1947(3)

[a] These values are reported by Alonso *et al.* (7).

respectively (16, 17). From the values of the spectroscopic splitting factor (g) and total angular momentum (J) of the Nd^{3+} ion, $\mu_{Nd^{3+}}$ is calculated to be 3.62 (18). In Fig. 4, broken lines [1] and [2] indicate the theoretical values calculated in the cases of both the high-spin and the low-spin states of the Ni^{3+} ions; line [1] is the high-spin state with $(d\varepsilon)^5(d\gamma)^2$ and line [2] is the low-spin state with $(d\varepsilon)^6(d\gamma)^1$. From these results, it is obvious that the spin state of the Ni^{3+} ion changes from low to high at $\approx$480 K. The ionic radii of the Cr^{3+} ion and the Ni^{3+} ion (low-spin state) with a coordination number (CN) of 6 are 0.0615 and 0.056 nm, respectively (5). Therefore, it is considered that both the a- and c-axes are strongly affected by the (Cr,Ni)–O(2) distance and the angle for (Cr,Ni)–O(2)–(Cr,Ni). On the other hand, the b-axis is affected by the angle for (Cr,Ni)–O(1)–(Cr,Ni).

The relative density of sintered $Nd(Cr_{1-x}Ni_x)O_3$ calculated from the observed density and the theoretical density was 0.86–0.92. Figure 5 shows the relationship between the logarithm of the electrical resistivity ($\log\rho$) of $Nd(Cr_{1-x}Ni_x)O_3$ and the reciprocal temperature ($1000/T$). $\log\rho$ at room temperature decreases with increasing x. The $\log\rho$–$1000/T$ curves are linear and have the deflection points at $\approx$570 K ($x = 0.0$) and $\approx$500 K ($0.2 \le x \le 0.6$). The deflection points are shown as arrows in Fig. 5. It is considered that the deflection points in the $\log\rho$–$1000/T$ curves correspond to the deflection points in the $1/\chi$–T curves. Activation energies, E_a ($300 \le T \le 500$ K) and

TABLE 3
Angles for (Cr,Ni)–O–(Cr,Ni) of $Nd(Cr_{1-x}Ni_x)O_3$

x	(Cr,Ni)–O(1)–(Cr,Ni) (deg)	(Cr,Ni)–O(2)–(Cr,Ni) (deg)
0.0	153.4(18)	154.2(11)
0.2	152.4(16)	154.8(10)
0.4	152.4(15)	154.8(9)
0.6	155.1(19)	155.5(12)
1.0[a]	157.4(2)	156.8(5)

[a] These values are reported by Alonso *et al.* (7).

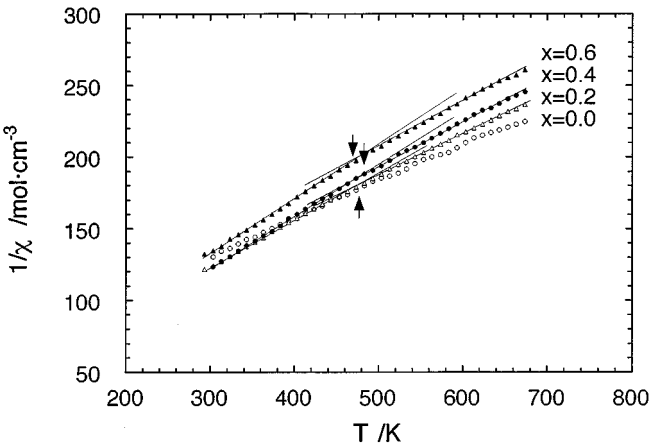

FIG. 3. Inverse magnetic susceptibility ($1/\chi$) vs temperature (T) for the system $Nd(Cr_{1-x}Ni_x)O_3$.

E_a ($500 \le T \le 900$ K), were calculated from the linear portions of the $\log\rho$–$1000/T$ curves. Figure 6 shows the relationship between E_a and the composition (x). E_a ($300 \le T \le 500$ K) decreases with increasing x in the range $0.0 \le x \le 0.2$, has a constant value ($\approx$0.13 eV) in the range $0.2 \le x \le 0.4$, and then decreases to 0.05 eV ($x = 0.6$). E_a ($500 \le T \le 900$ K) is slightly larger than E_a ($300 \le T \le 500$ K) in the range $0.2 \le x \le 0.6$. $Nd(Cr_{1-x}Ni_x)O_3$ is estimated to be metallic in the range $\approx 0.75 \le x \le 1.0$.

Figure 7 shows the relationship between the Seebeck coefficient (α) and temperature. α of $Nd(Cr_{1-x}Ni_x)O_3$

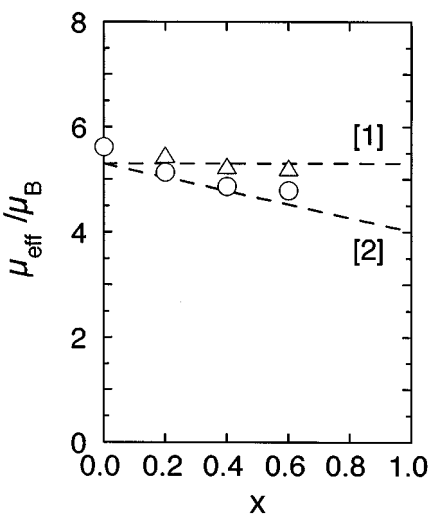

FIG. 4. Effective magnetic moment (μ_{eff}) vs composition (x) for the system $Nd(Cr_{1-x}Ni_x)O_3$: (○) observed μ_{eff} at $300 \le T \le 480$ K; (△) observed μ_{eff} at $480 \le T \le 650$ K. Broken lines [1] and [2] indicate the theoretical values calculated in the cases of both the high-spin and the low-spin states of the Ni^{3+} ion; line [1] is the high-spin state with $(d\varepsilon)^5(d\gamma)^2$ and line [2] is the low-spin state with $(d\varepsilon)^6(d\gamma)^1$.

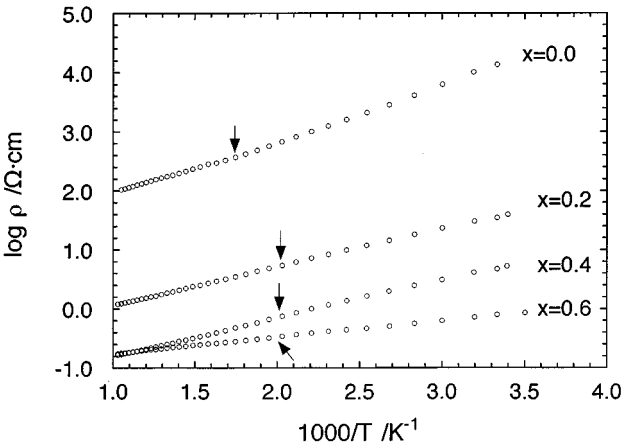

FIG. 5. Logarithm of the electrical resistivity ($\log \rho$) vs $1000/T$ for the system $Nd(Cr_{1-x}Ni_x)O_3$.

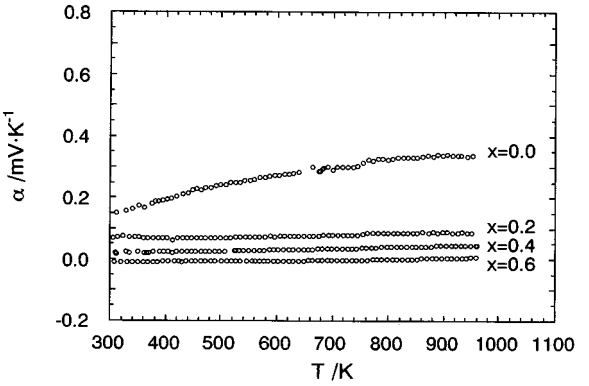

FIG. 7. Seebeck coefficient (α) vs temperature (T) for the system $Nd(Cr_{1-x}Ni_x)O_3$.

($0.0 \leq x \leq 0.4$) is positive, while α of $Nd(Cr_{0.4}Ni_{0.6})O_3$ ($x = 0.6$) changes from negative to positive at ≈ 800 K. α at 300 K is 0.149 ($x = 0.0$), 0.069 ($x = 0.2$), 0.021 ($x = 0.4$), and -0.001 mV/K ($x = 0.6$). With increasing temperature, α of $NdCrO_3$ ($x = 0.0$) increases gradually to ≈ 0.337 mV/K at 953 K. Although α of $Nd(Cr_{1-x}Ni_x)O_3$ ($x = 0.2$ and 0.4) also increases slightly with increasing temperature, the rate of increase (α/T) is very little in comparison with α/T of $NdCrO_3$ ($x = 0.0$). From these results, it is obvious that $Nd(Cr_{1-x}Ni_x)O_3$ ($0.0 \leq x \leq 0.4$) is a p-type semiconductor, while $Nd(Cr_{0.4}Ni_{0.6})O_3$ ($x = 0.6$) changes from an n-type to a p-type semiconductor at ≈ 800 K. To explain the temperature independence of α, Tuller and Nowick proposed an equation for a hopping mechanism involving a fixed number of carriers (19). Under the assumption that all other interaction effects are negligible, the following equation is obtained:

$$\alpha = \pm \frac{k}{e}\left\{\ln \beta\left(\frac{1-c}{c}\right) + \frac{S_T^*}{k}\right\}. \qquad [2]$$

Here S_T^* is the vibration entropy and is small enough to be negligible. β is a degeneracy factor; for the case of $\beta = 1$, Eq. [2] is often referred to as the "Heikes formula" (19). c is the fraction of sites which contain the electron,

$$c = \frac{n}{N}, \qquad [3]$$

where n is the number of carriers and N is the number of available sites per unit volume (V). V is easily calculated from the cell constants as shown in Table 1. Since there are four sites in the orthorhombic perovskite-type unit cell, N is expressed as $N = 4/V$. By substituting Eq. [3] into Eq. [2], n is obtained

$$n = \frac{4}{V}\left\{\frac{1}{\exp(\pm \alpha e/k) + 1}\right\}, \qquad [4]$$

and is calculated from α and N. n at 300 K is 8.74×10^{21} to 8.84×10^{21} and independent of x. The mobility (μ) is given by

$$\mu = \frac{\sigma}{en}, \qquad [5]$$

where σ is the electrical conductivity. Table 4 shows V, α, ρ, n, and μ at 300 K. μ at 300 K increases with increasing x.

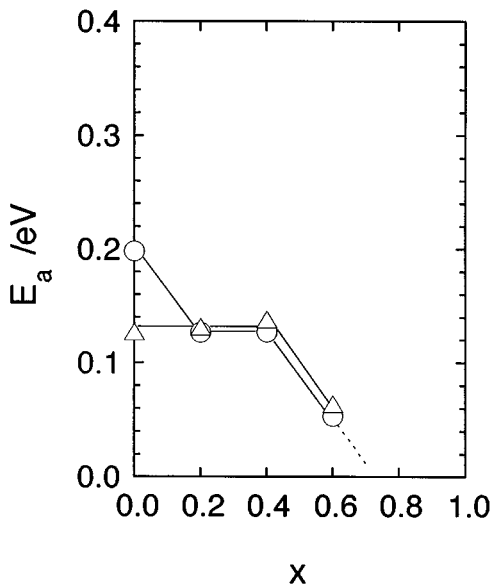

FIG. 6. Activation energy (E_a) vs composition (x) for the system $Nd(Cr_{1-x}Ni_x)O_3$: (○) E_a at $300 \leq T \leq 500$ K, (△) E_a at $500 \leq T \leq 900$ K.

TABLE 4

Cell Volume (V), Seebeck Coefficient (α), Electrical Resistivity (ρ), Number of Carriers (n), and Mobility (μ) at 300 K of $Nd(Cr_{1-x}Ni_x)O_3$

x	V (nm^3)	α ($V \cdot K^{-1}$)	ρ ($\Omega \cdot cm$)	n	μ ($cm^2 \cdot V^{-1} \cdot S^{-1}$)
0.0	0.2285	1.49×10^{-4}	1.36×10^{4}	8.74×10^{21}	5.24×10^{-8}
0.2	0.2286	6.90×10^{-5}	3.51×10^{1}	8.75×10^{21}	2.03×10^{-5}
0.4	0.2279	2.10×10^{-5}	4.75	8.77×10^{21}	1.50×10^{-4}
0.6	0.2262	-1.00×10^{-6}	0.79	8.84×10^{21}	8.94×10^{-4}

From these results, it is considered that μ dominates the electrical conductivity of $Nd(Cr_{1-x}Ni_x)O_3$ at room temperature.

The $(Cr,Ni)O_6$ octahedron in $Nd(Cr_{1-x}Ni_x)O_3$ connects with O(1) or O(2) of the other $(Cr,Ni)O_6$ octahedron. There are two kinds of cation–anion–cation overlap in $Nd(Cr_{1-x}Ni_x)O_3$; one is an overlap (π-bonding) between the cation $d\varepsilon$ and oxygen p_π orbitals, and the other is an overlap (σ-bonding) between the cation $d\gamma$ and oxygen p_σ orbitals. Goodenough reported that three $3d$ electrons of the Cr^{3+} ion in $LaCrO_3$ are all localized and the Fermi level lies between the filled t_{2g}^* level and the narrow e_g^* level (20). Since the (Cr,Ni)–O(1 and 2) distances are almost independent of x in the range $0.0 \le x \le 0.4$, the cation–anion–cation overlap depends on the angles for (Cr,Ni)–O(1 and 2)–(Cr,Ni). The decrease in the angles for (Cr,Ni)–O(1)–(Cr,Ni) makes π-bonding stronger, and the increase in the angle for (Cr,Ni)–O(2)–(Cr,Ni) makes σ-bonding stronger. In the range $0.4 \le x \le 0.6$, the (Cr,Ni)–O(1 and 2) distances decrease with increasing x. Therefore, the increase in the cation–anion–cation overlap makes $\log \rho$ decrease, and the cation–anion–cation overlap integrals (Δ_{cac}^{π} for π-bonding and for Δ_{cac}^{σ} for σ-bonding) are less than the critical overlap integral (Δ_C); $\Delta_{cac}^{\pi} < \Delta_{cac}^{\sigma} < \Delta_c$ (21). As shown in Fig. 4, the spin state of the Ni^{3+} ion changes from low to high at $\approx$480 K. Since the ionic radius of the Ni^{3+} ion with the high-spin state is larger than that of the Ni^{3+} ion with the low-spin state (5), it is considered that the change of the spin state of the Ni^{3+} ion lengthens the (Cr,Ni)–O distance. Therefore, the decrease of the cation–anion–cation overlap makes the slight increase in E_a above $\approx$500 K. These results indicate that the cation–anion–cation overlap is strongly affected by the spin state of the Ni^{3+} ion, the (Cr,Ni)–O distance, and the angle for (Cr,Ni)–O–(Cr,Ni).

CONCLUSION

Orthorhombic perovskite-type $Nd(Cr_{1-x}Ni_x)O_3$ ($0.0 \le x \le 0.6$) was synthesized in a flow of pure oxygen gas by using $Nd(NO_3)_3 \cdot 6H_2O$, Cr_2O_3, and $Ni(CH_3COO)_2 \cdot 4H_2O$ powders. Magnetic measurement indicates that the spin state of the Ni^{3+} ion changes from low to high at $\approx$480 K. $Nd(Cr_{1-x}Ni_x)O_3$ ($0.0 \le x \le 0.4$) is a p-type semiconductor, while $Nd(Cr_{0.4}Ni_{0.6})O_3$ ($x = 0.6$) is an n-type semiconductor. The $\log \rho$–$1000/T$ curves of $Nd(Cr_{1-x}Ni_x)O_3$ ($0.2 \le x \le 0.6$) have deflection points at $\approx$500 K, which correspond to the deflection points in the $1/\chi$–T curves. From these results, it is obvious that the spin state of the Ni^{3+} ion strongly affects the electrical properties.

ACKNOWLEDGMENT

The author expresses his thanks to Dr. H. Kido, Osaka Municipal Technical Institute, for the magnetic measurements.

REFERENCES

1. T. Arakawa, S. Tsuchi-Ya, and J. Shiokawa, *Mater. Res. Bull.* **16,** 97 (1981).
2. J. B. Goodenough and J. M. Longo, *in* "Landolt-Bornstein, Numerical Data and Functional Relationships in Science and Technology. Magnetic and Other Properties of Oxides and Related Compounds," New Series, Group 3, Vol. 4 (K. H. Hellwege, Ed.), p. 228. Springer-Verlag, New York, 1971.
3. G. V. S. Rao, B. M. Wanklyn, and C. N. R. Rao, *J. Phys. Chem. Solids* **32,** 345(1971).
4. H. Taguchi, M. Nagao, and Y. Takeda, *J. Solid State Chem.* **114,** 236 (1995).
5. R. D. Shannon, *Acta Crystallogr. A* **32,** 751 (1976).
6. W. Gordy and J. O. Thomas, *J. Chem. Phys.* **24,** 439 (1956).
7. J. Alonso, M. J. Martínez-Lope, and M. A. Hidalgo, *J. Solid State Chem.* **116,** 146 (1995).
8. G. Frand, O. Bohnke, P. Lacorre, L. Fourquet, A. Carré, B. Eid, J. B. Théobald, and A. Gire, *J. Solid State Chem.* **120,** 157 (1995).
9. M. J. Sayagués, M. Vallet-Regí, A. Caneiro, and M. Gnzález-Calbet, *J. Solid State Chem.* **110,** 295 (1994).
10. J. L. Gracía-Munoz, J. Rodríguez-Carvajal, P. Lacorre, and J. B. Torrance, *Phys. Rev.* **46,** 4414 (1992).
11. X. Granados, J. Fontcuberta, X. Obradors, Ll. Manosa, and J. B. Torrance, *Phys. Rev.* **48,** 11666 (1993).
12. F. Izumi, "The Rietveld Method," p. 236. Oxford University Press, Oxford, 1993.
13. H. Taguchi, H. Yoshioka, D. Matsuda, and M. Nagao, *J. Solid State Chem.* **104,** 460 (1993).
14. T Kobayashi, H. Takizawa, T. Endo, T. Sato, M. Shimada, H. Taguchi, and M. Nagao, *J. Solid State Chem.* **92,** 116 (1991).
15. K. R. Poeppelmeier, M. E. Leonowicz, J. C. Scanlon, and W. B. Yelon, *J. Solid State Chem.* **45,** 71 (1982).
16. T. Shin-Ike, T. Sakai, G. Adachi, and J. Shiokawa, *Mater. Res. Bull.* **12,** 831 (1977).
17. H. Taguchi, *J. Solid State Chem.* **118,** 367 (1995).
18. A. J. Dekker, "Solid State Physics," p. 450. Prentice-Hall, New York, 1970.
19. H. L. Tuller and A. S. Nowick, *J. Phys. Chem. Solids* **38,** 859 (1977).
20. J. B. Goodenough, *J. Appl. Phys.* **37,** 1415 (1966).
21. J. B. Goodenough, *Czech. J. Phys.* **B17,** 304 (1967).